Neutron Capture Cross Section Measurement of ^{151}Sm at the CERN Neutron Time of Flight Facility (n_TOF)

U. Abbondanno,[14] G. Aerts,[7] F. Alvarez-Velarde,[20] H. Álvarez-Pol,[24] S. Andriamonje,[7] J. Andrzejewski,[33] G. Badurek,[1] P. Baumann,[6] F. Bečvář,[31] J. Benlliure,[24] E. Berthoumieux,[7] F. Calviño,[25] D. Cano-Ott,[20] R. Capote,[29] P. Cennini,[4] V. Chepel,[17] E. Chiaveri,[4] N. Colonna,[13] G. Cortes,[25] D. Cortina,[24] A. Couture,[29] J. Cox,[29] S. Dababneh,[8] M. Dahlfors,[4] S. David,[5] R. Dolfini,[15] C. Domingo-Pardo,[21] I. Duran,[24] M. Embid-Segura,[20] L. Ferrant,[5] A. Ferrari,[4] R. Ferreira-Marques,[17] H. Frais-Koelbl,[3] W. Furman,[18] I. Goncalves,[30] R. Gallino,[36] E. Gonzalez-Romero,[20] A. Goverdovski,[19] F. Gramegna,[12] E. Griesmayer,[3] F. Gunsing,[7] B. Haas,[32] R. Haight,[27] M. Heil,[8,*] A. Herrera-Martinez,[4] S. Isaev,[5] E. Jericha,[1] F. Käppeler,[8] Y. Kadi,[4] D. Karadimos,[9] M. Kerveno,[6] V. Ketlerov,[19] P. Koehler,[28] V. Konovalov,[18] M. Krtička,[31] C. Lamboudis,[10] H. Leeb,[1] A. Lindote,[17] I. Lopes,[17] M. Lozano,[29] S. Lukic,[6] J. Marganiec,[33] S. Marrone,[13] J. Martinez-Val,[22] P. Mastinu,[12] A. Mengoni,[4] P. M. Milazzo,[14] A. Molina-Coballes,[21] C. Moreau,[14] M. Mosconi,[8] F. Neves,[17] H. Oberhummer,[1] S. O'Brien,[29] J. Pancin,[7] T. Papaevangelou,[4] C. Paradela,[24] A. Pavlik,[2] P. Pavlopoulos,[34] J. M. Perlado,[22] L. Perrot,[7] M. Pignatari,[36] R. Plag,[8] A. Plompen,[16] A. Plukis,[7] A. Poch,[25] A. Policarpo,[17] C. Pretel,[25] J. Quesada,[23] S. Raman,[28,†] W. Rapp,[8] T. Rauscher,[26] R. Reifarth,[27] M. Rosetti,[11] C. Rubbia,[15] G. Rudolf,[6] P. Rullhusen,[16] J. Salgado,[30] J. C. Soares,[30] C. Stephan,[5] G. Tagliente,[13] J. Tain,[21] L. Tassan-Got,[5] L. Tavora,[30] R. Terlizzi,[13] G. Vannini,[35] P. Vaz,[30] A. Ventura,[11] D. Villamarin,[20] M. C. Vincente,[20] V. Vlachoudis,[4] F. Voss,[8] H. Wendler,[4] M. Wiescher,[29] and K. Wisshak[8]

(n_TOF Collaboration)

[1]*Atominstitut der Österreichischen Universitäten, Technische Universität Wien, Wien, Austria*
[2]*Institut für Isotopenforschung und Kernphysik, Universität Wien, Austria*
[3]*Fachhochschule Wiener Neustadt, Wiener Neustadt, Austria*
[4]*CERN, Geneva, Switzerland*
[5]*Centre National de la Recherche Scientifique/IN2P3-IPN, Orsay, France*
[6]*Centre National de la Recherche Scientifique/IN2P3-IReS, Strasbourg, France*
[7]*CEA/Saclay-DSM, Gif-sur-Yvette, France*
[8]*Institut für Kernphysik, Forschungszentrum Karlsruhe GmbH (FZK), Karlsruhe, Germany*
[9]*University of Ioannina, Ioannina, Greece*
[10]*Aristotle University of Thessaloniki, Thessaloniki, Greece*
[11]*ENEA, Bologna, Italy*
[12]*Laboratori Nazionali di Legnaro, Legnaro, Italy*
[13]*Istituto Nazionale di Fisica Nucleare, Bari, Italy*
[14]*Istituto Nazionale di Fisica Nucleare, Trieste, Italy*
[15]*Università degli Studi Pavia, Pavia, Italy*
[16]*CEC-JRC-IRMM, Geel, Belgium*
[17]*LIP-Coimbra & Departamento de Fisica da Universidade de Coimbra, Coimbra, Portugal*
[18]*Joint Institute for Nuclear Research, Frank Laboratory of Neutron Physics, Dubna, Russia*
[19]*Institute of Physics and Power Engineering, Kaluga region, Obninsk, Russia*
[20]*Centro de Investigaciones Energeticas Medioambientales y Technologicas, Madrid, Spain*
[21]*Consejo Superior de Investigaciones Cientificas, University of Valencia, Valencia, Spain*
[22]*Universidad Politecnica de Madrid, Madrid, Spain*
[23]*Universidad de Sevilla, Sevilla, Spain*
[24]*Universidade de Santiago de Compostela, Santiago de Compostela, Spain*
[25]*Universitat Politecnica de Catalunya, Barcelona, Spain*
[26]*Department of Physics and Astronomy, University of Basel, Basel, Switzerland*
[27]*Los Alamos National Laboratory, Los Alamos, New Mexico 87545, USA*
[28]*Physics Division, Oak Ridge National Laboratory, Oak Ridge, Tennessee 37831, USA*
[29]*University of Notre Dame, Notre Dame, Indiana 46556, USA*
[30]*Instituto Tecnológico e Nuclear, Lisbon, Portugal*
[31]*Charles University, Prague, Czech Republic*
[32]*Centre National de la Recherche Scientifique/IN2P3-CENBG, Bordeaux, France*
[33]*University of Lodz, Lodz, Poland*
[34]*Pôle Universitaire Léonard de Vinci, Paris La Défense, France*
[35]*Dipartimento di Fisica, Università di Bologna, and Sezione INFN di Bologna, Bologna, Italy*

 0031-9007/04/93(16)/161103(5)$22.50

[36]*Dipartimento di Fisica Generale, Università di Torino, and Sezione INFN di Torino, I-10125 Torino, Italy*
(Received 3 May 2004; published 14 October 2004)

The ^{151}Sm$(n, \gamma)^{152}$Sm cross section has been measured at the spallation neutron facility n_TOF at CERN in the energy range from 1 eV to 1 MeV. The new facility combines excellent resolution in neutron time-of-flight, low repetition rates, and an unsurpassed instantaneous luminosity, resulting in rather favorable signal/background ratios. The ^{151}Sm cross section is of importance for characterizing neutron capture nucleosynthesis in asymptotic giant branch stars. At a thermal energy of kT = 30 keV the Maxwellian averaged cross section of this unstable isotope ($t_{1/2}$ = 93 yr) was determined to be 3100 ± 160 mb, significantly larger than theoretical predictions.

DOI: 10.1103/PhysRevLett.93.161103 PACS numbers: 25.40.Lw, 26.20.+f, 27.70.+q, 97.10.Cv

The neutron capture cross section of ^{151}Sm has important implications in nuclear astrophysics for constraining the temperature during He shell burning in asymptotic giant branch (AGB) stars, and for advanced reactor concepts, where it determines the transmutation rate of this long-lived fission product. This Letter describes the measurement and the astrophysical aspects.

The unstable isotope ^{151}Sm is one of the key nuclei for characterizing nucleosynthesis in the slow neutron capture process (*s* process) related to He shell burning in thermally pulsing low mass stars during their AGB phase. The *s* process is producing about half of the isotopic abundances in the mass range between Fe and Bi. In this context, ^{151}Sm acts as a branching point in the neutron capture flow at $A = 151$ (Fig. 1). The branching is defined by the abundances of ^{152}Gd and ^{154}Gd, which are considered to be of pure *s*-process origin, since they are shielded from possible *r*-process contributions by their stable Sm isobars. The partition of the neutron capture chain reflects the competing neutron captures and β decays at the unstable branching points ^{151}Sm and ^{154}Eu. The relevant neutron capture and β-decay rates are determined by the neutron density and temperature at the site of the *s* process. Under stellar conditions, the β-decay rates of both branching points are significantly increased compared to their terrestrial values due to the population of low lying states in the intense stellar photon bath [1], a feature that allows the interpretation of this branching as a potential *s*-process thermometer.

For ^{151}Sm the branching factor is defined by the σN_s values of ^{152}Gd, which is partially bypassed, and of ^{150}Sm, which represents the entire reaction flow,

$$f_\beta = \frac{(\sigma N_s)_{^{152}\mathrm{Gd}}}{(\sigma N_s)_{^{150}\mathrm{Sm}}} = \frac{\lambda_{\beta(^{151}\mathrm{Sm})}}{\lambda_{\beta(^{151}\mathrm{Sm})} + \lambda_{n(^{151}\mathrm{Sm})}},$$

where σ is the Maxwellian averaged cross section of the corresponding isotope, N_s is the *s*-process abundance, while λ_β and λ_n denote the β-decay and neutron capture rates. The neutron capture rate $\lambda_n = v_T n_n \langle\sigma\rangle$ is determined by the thermal velocity of the neutrons, the neutron density, and the cross section averaged over the stellar spectrum. For obtaining $\langle\sigma\rangle$ at *s*-process temperatures, the cross section has to be measured in the neutron energy interval from 0.3 to 300 keV.

In the so-called classical approach, where the neutron density and temperature are assumed to be constant in time, this equation can be used to derive an effective stellar decay rate of ^{151}Sm. If all other quantities are known to sufficient accuracy, the temperature at the stellar site can be derived from the temperature dependence of the ^{151}Sm half-life, which decreases from the terrestrial value of 93 yr to a few years in the He burning [1] shell of low mass AGB stars. This simple picture becomes more complex as more realistic stellar models of the *s* process are considered, which account for the fact that He shell burning in low mass AGB stars occurs in a repeated sequence of alternating H burning and He burning episodes. These episodes are characterized by different neutron sources, operating at different temperature and time scales and need to be treated with a comprehensive reaction network. Independent of the particular *s*-process model, the branching at ^{151}Sm can be analyzed only with the proper nuclear physics input. Apart from the temperature-dependent half-life, the unknown capture cross section of the radioactive branching point

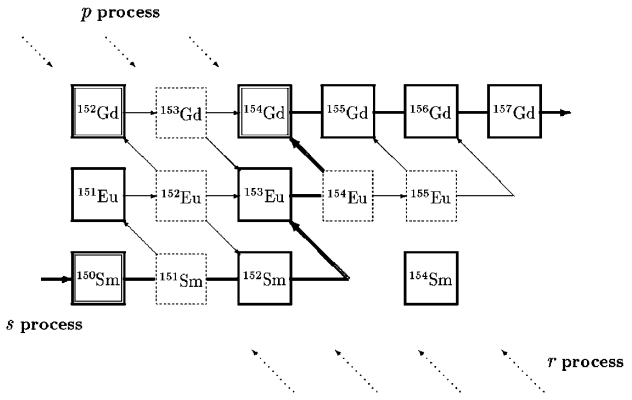

FIG. 1. The *s*-process network in the mass region of ^{151}Sm. Branchings of the reaction path occur at ^{151}Sm, ^{152,154,155}Eu, and ^{153}Gd. The branching effect at ^{152}Eu is completely dominated by the β-decay rate, which is strongly enhanced at stellar temperatures. Branching point nuclei and *s*-only isotopes are indicated by dashed and double boxes, respectively.

isotope ^{151}Sm represents a persisting uncertainty for the analysis of this branching. Theoretical predictions, obtained with the Hauser-Feshbach statistical model, were found to range between 1500 and 2800 mb [2].

The (n, γ) cross section of ^{151}Sm has not been measured so far partly because of the sample activity, which was 156 GBq in the present case (Table II). This problem could be mastered with the unique features of the n_TOF facility, which combines low background, excellent resolution, high instantaneous neutron flux, and a very low duty factor [3]. In a parallel experiment at Karlsruhe, which reported excellent agreement in the energy range between 3 and 225 keV, the background due to the activity of the sample could be handled by using the 4π BaF_2 detector [4].

At n_TOF, neutrons are generated by spallation reactions induced by a pulsed 20 GeV proton beam on a Pb target block. The neutrons are slowed down in the lead and moderated in the surrounding 5 cm thick layer of cooling water. An evacuated neutron flight path with collimators at 135 and 175 m leads to the measuring station at a distance of 185 m from the lead target. Backgrounds due to fast charged particles are suppressed by heavy concrete and iron shieldings and by a sweeping magnet at 145 m. The main parameters are summarized in Table I (for details, see Refs. [3,5]).

The experimental setup [6] consists of two C_6D_6 detectors with minimized neutron sensitivity [7], placed perpendicular to the neutron beam at a distance of about 3 cm from the beam axis. The background due to scattering of in-beam γ rays was reduced by placing the detectors 9 cm upstream of the sample. The ^{151}Sm was encapsulated in a thin titanium can for safe handling of the highly radioactive sample. The additional gold, carbon, and lead samples for flux and background measurements were canned in the same way (Table II). The relative neutron flux was measured 1.5 m upstream of the capture samples with a flux monitor consisting of a thin layer of ^{6}Li surrounded by four Si detectors outside the neutron beam [8]. Figure 2 shows the capture yield of the ^{151}Sm sample and the overall background.

The main steps of data analysis consist of repeated energy calibrations with radioactive sources, subtraction of the overall background, the calculation of the pulse height weighting functions, and the definition of the neutron flux via the Au runs. The proper subtraction of the ambient background was verified by the complete disappearance of the Ti resonances around 10 keV, which are clearly visible in Fig. 2. The adopted pulse height threshold was defined via software and corresponds to a γ-ray energy of 200 keV. For all samples the weighting functions were obtained from simulations of the detector response performed with GEANT-3.21 and GEANT-4 [10], using a detailed model of the experiment setup, including detector resolution and pulse height threshold.

The weighted capture yields per bunch are

$$\sum R_i W_i = E_c \int \Phi(E) Y(E) dE,$$

where $\Phi(E)$ and $Y(E)$ are, respectively, the neutron flux and measured yields per energy interval, and E_c is the energy of the γ-ray cascade.

The inset in Fig. 2 shows an R-matrix fit of the ^{151}Sm resonances between 490 and 550 eV with the SAMMY code [9]. Compared to previous data from a total cross section measurement [11] the superior resolution of the n_TOF facility allows one to extend the resolved resonance region up to about 1 keV, a factor of 5 higher than before.

The cumulative number of levels deduced from the resonance analysis are plotted in Fig. 3 versus neutron energy. With the assumption of Ref. [11] that all levels are s-wave resonances, the deduced average level spacing $\langle D \rangle = 1.48 \pm 0.04$ eV and the neutron strength function $S_0 = (3.87 \pm 0.20)10^{-4}$ are consistent with but more accurate than the values reported in Ref. [11] since the present measurement was performed with significantly improved sensitivity and resolution, which provides a complete resonance analysis up to $E_n = 400$ eV. This is important in view of expected nuclear structure effects in ^{152}Sm [12].

In the unresolved resonance region, the background due to scattered neutrons, measured with the carbon sample, was found to be negligible, whereas the Au spectrum had to be corrected for the background produced by in-beam γ rays measured with the Pb sample. This background was carefully evaluated by additional runs with W and Al filters in the beam. While negligible for the empty Ti can, the carbon sample, and the Sm_2O_3 sample, significant corrections for in-beam γ rays had to be made for the gold and lead samples [3].

The overall 5% uncertainty of the present data was evaluated by a thorough analysis of the various corrections and backgrounds. The main sources of uncertainty are related to the neutron flux (3%), the weighting functions (2%), and the background subtraction (3%).

TABLE I. Main features of the n_TOF facility [3].

Parameter	Comments
Proton beam	20 GeV, pulse width 7 ns, repetition rate 0.4 Hz, intensity 7×10^{12} p/pulse
Neutron beam	300 n/p, energies from 0.1 eV to 250 MeV, flux at 185 m $\approx 10^5$ n/pulse/energy decade, resolution $\Delta E/E = 10^{-3}$ at 30 keV, neutron filters for background definition

TABLE II. Sample parameters[a] and composition.

	^{151}Sm	^{197}Au	Carbon	Lead
Mass (mg)	206.4	1480	230	950
Chemical form	Sm_2O_3	Metal	Powder	Metal
Enrichment (%)	89.9[b]	100	Natural	Natural

[a]All samples: 10 mm in diameter; encapsulated in 0.2 mm Ti.
[b]Main isotopic impurities: ^{150}Sm, ^{152}Sm, ^{151}Eu.

From the cross section, $\sigma(E_n)$, Maxwellian averaged cross sections were determined for the relevant stellar range of thermal energies between 5 and 30 keV. Figure 4 shows a comparison of the present value of 3100 ± 160 mb for $kT = 30$ keV with previous predictions based on statistical model calculations [2]. In this case all theoretical results are smaller than the experimental value, in contrast to the neighboring branching point ^{147}Pm, where the cross section was always overestimated [13].

Recent analyses of the branchings at $A = 148$, 151, 154, and 163 using the classical s-process approach [14] have shown that it is difficult to achieve a consistent description of the isotopic abundances, although the cross sections of the involved stable isotopes are accurately known [2]. By the present measurement of the ^{151}Sm cross section a crucial uncertainty of such analyses could be removed. For the classical approach, however, the larger value in combination with the high neutron density of Ref. [13] would imply s-process temperatures in excess of $T_8 = 4$, completely inconsistent with realistic conditions for stellar He burning.

A possible solution of these problems is obtained by treating these branchings in the framework of the more complex scenario related to the s process in recurrent thermal instabilities in the AGB phase of 1.5 to 3 $M_\odot$ mass stars [15–17]. In this model, about 95% of the neutron irradiation occurs via the ^{13}C$(\alpha, n)^{16}$O reaction

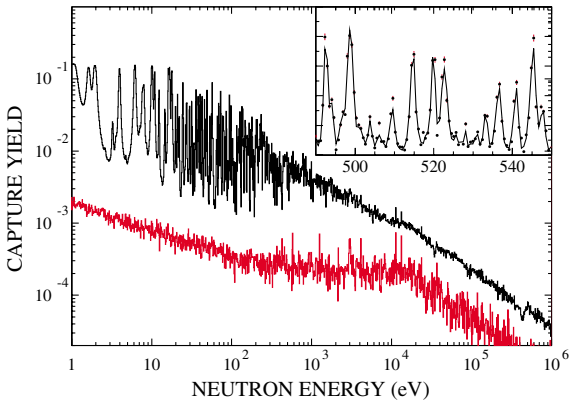

FIG. 2 (color online). Capture yields for ^{151}Sm plotted with the overall background. The inset shows a SAMMY fit [9] of the resonances between 490 and 550 eV.

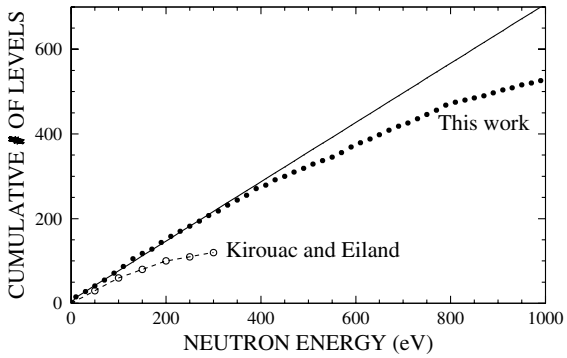

FIG. 3. Cumulative number of levels at the neutron separation energy of ^{152}Sm fitted at energies below 400 eV.

between thermal instabilities at comparably low temperatures of $T_8 = 1$ (temperature in units of 10^8 K). In this phase, the decay of ^{151}Sm is yet too slow for a sufficient production of ^{152}Gd. During thermal instabilities, however, temperatures of $T_8 = 2.5$–2.8 are reached for a few years, resulting in a second neutron burst due to the marginal activation of the ^{22}Ne$(\alpha, n)^{25}$Mg reaction. At these higher temperatures, the decay of ^{151}Sm is enhanced, resulting eventually in a ^{152}Gd abundance, which accounts for 71% of the solar value. The missing abundance component must be ascribed to the p process, yielding $N_p(^{152}\text{Gd}) = 1.9 \times 10^{-4}$ (relative to Si $= 10^6$, [18]). This interpretation is supported by the abundances of the nearest p-only isotopes ^{156}Dy and ^{158}Dy (2.36×10^{-4} and 3.9×10^{-4}, respectively). Hence, the temperature and neutron density profiles of the invoked s-process model yield a consistent description of the abundance pattern in the Sm-Eu-Gd region, although the uncertainty in the temperature dependence of the ^{151}Sm half-life represents a remaining difficulty of the present analysis. This problem could be further reduced via analyses of other branchings, e.g., at $A = 176$ [19].

In conclusion, the successful measurement of the ^{151}Sm$(n, \gamma)^{152}$Sm cross section illustrates the excellent performance of the new spallation neutron facility n_TOF at CERN, which covers a wide energy range with very good resolution, high neutron flux, low backgrounds, and a favorable duty factor. The combination of

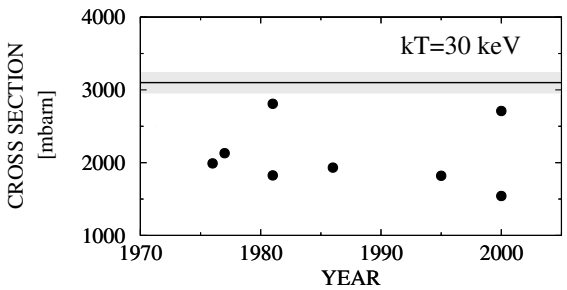

FIG. 4. Maxwellian averaged (n, γ) cross section of ^{151}Sm (shaded band) and previous calculations (symbols) [2].

these features is quite unique and provides a promising basis for a broad experimental program directed towards applications in astrophysics, advanced nuclear technologies, and basic nuclear physics.

This work was partly supported by the EC under contract FIKW-CT-2000-00107 and by the funding agencies of the participating institutes.

*Corresponding author at Institut für Kernphysik, Forschungszentrum Karlsruhe, Postfach 3640, D-76021 Karlsruhe, Germany.
Electronic address: michael.heil@ik.fzk.de
†Deceased.

[1] K. Takahashi and K. Yokoi, At. Data Nucl. Data Tables **36**, 375 (1987).
[2] Z. Bao *et al.*, At. Data Nucl. Data Tables **76**, 70 (2000).
[3] U. Abbondanno *et al.*, CERN Report No. CERN-SL-2002-053 ECT, 2003.
[4] K. Wisshak *et al.*, Forschungszentrum Karlsruhe Report No. FZKA 6996, 2004.
[5] C. Borcea *et al.*, Nucl. Instrum. Methods Phys. Res., Sect. A **513**, 524 (2003).
[6] S. Marrone *et al.*, in *Nuclear Data for the Transmutation of Nuclear Waste*, edited by A. Kelic and K. H. Schmidt, ISBN 3-00-012276-1, http://www-w2k.gsi.de/tramu/, 2003.
[7] R. Plag *et al.*, Nucl. Instrum. Methods Phys. Res., Sect. A **496**, 425 (2003).
[8] S. Marrone *et al.*, Nucl. Instrum. Methods Phys. Res., Sect. A **517**, 389 (2004).
[9] N. Larson, Oak Ridge National Laboratory Report No. ORNL/TM-9179/R5, 2000.
[10] U. Abbondanno *et al.*, Nucl. Instrum. Methods Phys. Res., Sect. A **521**, 454 (2004).
[11] G. Kirouac and H. Eiland, Phys. Rev. C **11**, 895 (1975).
[12] R. F. Casten and N.V. Zamfir, Phys. Rev. Lett. **87**, 052503 (2001).
[13] R. Reifarth *et al.*, Astrophys. J. **582**, 1251 (2003).
[14] J. Best *et al.*, Phys. Rev. C **64**, 15 801 (2001).
[15] O. Straniero *et al.*, Astrophys. J. **440**, L85 (1995).
[16] O. Straniero *et al.*, Astrophys. J. **478**, 332 (1997).
[17] R. Gallino *et al.*, Astrophys. J. **497**, 388 (1998).
[18] E. Anders and N. Grevesse, Geochim. Cosmochim. Acta **53**, 197 (1989).
[19] C. Doll *et al.*, Phys. Rev. C **59**, 492 (1999).